Boston University

OpenBU **http://open.bu.edu**

BU Open Access Articles BU Open Access Articles

2022-05-16

Dependence of nonlinear effects on whistler-mode wave bandwidth and amplitude: a perspective from diffusion coefficients

L. Gan, W. Li, Q. Ma, A. Artemyev, J. Albert. 2022. "Dependence of nonlinear effects on whistler-mode wave bandwidth and amplitude: A perspective from diffusion coefficients" Journal of Geophysical Research: Space Physics. https://doi.org/10.1029/2021JA030063

https://hdl.handle.net/2144/46487

Downloaded from DSpace Repository, DSpace Institution's institutional repository

Dependence of Nonlinear Effects on Whistler-Mode Wave Bandwidth and Amplitude: A Perspective from Diffusion Coefficients

L. Gan[1], W. Li[1], Q. Ma[1,2], A.V. Artemyev[3], and J. M. Albert[4]

[1]Center for Space Physics, Boston University, Boston, MA, USA.
[2]Department of Atmospheric and Oceanic Sciences, University of Los Angeles, CA, USA.
[3]Department of Earth, Planetary, and Space Sciences, University of Los Angeles, CA, USA.
[4]Air Force Research Laboratory, Kirtland Air Force Base, Albuquerque, NM, USA.

Corresponding authors: Wen Li, luckymoon761@gmail.com; Longzhi Gan, lzgan@bu.edu

Key Points:

- The maximum wave amplitude threshold for the applicability of quasilinear theory increases with increasing bandwidth.
- Electron diffusion acceleration due to intense broadband whistler-mode waves is limited by phase trapping trajectory along the field line.
- Interactions between intense whistler-mode waves and small pitch angle electrons limit the applicability of diffusion models.

Abstract

The electron resonant interaction with whistler-mode waves is characterized by transport in pitch angle-energy space. We calculate electron diffusion and advection coefficients (a simplified characterization of transport) for a large range of electron pitch angle and energy using test particle simulations. Nonlinear effects are analyzed by comparing the diffusion coefficients using test particle simulations and quasilinear theory, and by evaluating the advection rates. Dependence of nonlinear effects on the wave amplitude and bandwidth of whistler-mode waves is evaluated by running test particle simulations with a broad range of wave amplitude and bandwidth. The maximum amplitudes where the quasilinear approach is valid are found to increase with increasing bandwidth, from 50 pT for narrowband waves to 300 pT for broadband waves at *L*-shell of 6. Moreover, interactions between intense whistler-mode waves and small pitch angle electrons lead to large positive advection, which limits the applicability of diffusion-based models. This study demonstrates the parameter range of the applicability of quasilinear theory and diffusion model for different wave amplitudes and frequency bandwidths of whistler-mode waves, which is critical for evaluating the effects of whistler-mode waves on energetic electrons in the Earth's magnetosphere.

1. Introduction

Quasilinear (QL) theory has been widely used for modeling interactions between electromagnetic plasma waves and energetic electrons in the Earth's radiation belts. The theory assumes weak perturbations from the wave-particle resonances, and evaluates the long-term particle dynamics as diffusion processes (Kennel & Engelmann, 1966; Schulz & Lanzerotti, 2012). The full Vlasov equation is reduced to the Fokker-Planck equation, which uses diffusion coefficients to evaluate the rate of particle scattering due to plasma waves (Lyons et al., 1972; Lyons, 1974; Schulz & Lanzerotti, 1974) . When applied to the field of space physics, the diffusion coefficients are generally averaged along the unperturbed bounce trajectory, due to the inhomogeneous background magnetic fields (Albert, 2010; Le Queau & Roux, 1987; Karpman, 1974).

QL theory is commonly used in modeling the interactions between electrons and whistler-mode waves, which exhibit either discrete or broadband structures (e.g., Burtis & Helliwell, 1969; Burton and Holzer, 1974; Gao et al., 2014; Li et al., 2012). Although QL simulations successfully reproduced many observed electron dynamics (e.g., Albert et al., 2009; Drozdov et al., 2015; Glauert et al., 2014; Horne et al., 2005; Li et al., 2014; Ma et al., 2018; Shprits et al., 2009; Thorne et al., 2013; Xiao et al., 2009, 2010), observations have shown abundant large-amplitude and discrete whistler-mode waves including intense chorus waves, for which the QL theory may not be valid (Cattell et al., 2008; Cully et al., 2008; Tyler et al., 2019; Wilson et al., 2011; Zhang et al., 2019). Energetic electrons interacting with intense, monochromatic whistler-mode waves can experience nonlinear (NL) phase trapping through continuous resonance which leads to the fast acceleration, or phase bunching which leads to efficient decreases in electron energy (Albert, 1993, 2000; Bell, 1984; Bortnik et al., 2008; Demekhov et al., 2006; Inan et al., 1978; Karpman et al., 1975; Omura et al., 2007). Previous studies have indicated the potentially important contribution from these NL processes in the radiation belts (Agapitov et al., 2015; Bellan, 2013; Bortnik et al., 2008; Demekhov et al., 2009; Gan, et al., 2020a; Katoh & Omura, 2004; Katoh et al., 2008; Nunn & Omura, 2015; Vainchtein et al., 2018), especially for the fast acceleration of energetic electrons (Agapitov et al., 2014;

Hsieh & Omura, 2017; Mourenas et al., 2018; Omura et al., 2015; Summers & Omura, 2007), and rapid electron precipitation (Breneman et al., 2017; Hikishima et al., 2010; O'Brien et al., 2004; Shumko et al., 2018; Tsurutani et al., 2013). These studies are mostly focused on monochromatic waves, while statistical studies show that whistler-mode waves are commonly observed with finite bandwidths (Burton & Holzer, 1974; Crabtree et al., 2017; Gao et al., 2014; Santolík et al., 2003).

NL effects of whistler-mode waves with finite bandwidths and the implications on the applicability of QL theory are outstanding open questions under active investigations. Tao et al. (2012) compared the diffusion coefficients calculated from QL theory and test particle (TP) simulations using whistler-mode waves with different bandwidths and amplitudes. However, the threshold of wave amplitude and bandwidth in which QL theory agrees with TP simulations for electrons with a broad range of pitch angle and energy is not explored. Allanson et al. (2020) made the comparison using particle-in-cell simulations, but in the homogeneous background magnetic field. An et al. (2022) recently studied the NL effects of realistic chorus waves generated from particle-in-cell simulations, with inhomogeneous magnetic field. Furthermore, recent numerical and theoretical studies show that NL phase trapping, or anomalous phase bunching, can occur for electrons with small pitch angles (Albert et al., 2021; Artemyev et al., 2021; Gan et al., 2020b; Kitahara & Katoh, 2019). This finding could potentially limit the applicability of QL theory near the loss-cone, which is not addressed by previous studies.

In this paper, we compare the diffusion coefficients calculated from both TP and QL methods, for electrons with different initial energies and pitch angles. Whistler-mode waves with a broad range of bandwidths and amplitudes are adopted to perform simulations. The numerical results of these models are used to quantitatively analyze the dependence of NL effects on both the bandwidth and amplitude of whistler-mode waves.

2. Wave Models and Test Particle Simulations

2.1 Frequency Spectrum Models of Whistler-mode Waves

For all TP and QL simulations, wave frequency spectra are assumed to follow a Gaussian distribution $I(f) = I_0 * \exp\left(-\frac{(f-f_0)^2}{df^2}\right)$. Here $I(f)$ is the wave magnetic spectral density as a function of frequency (f); f_0 is the peak frequency set to 0.3 electron gyrofrequency at the magnetic equator (f_{ce}) for all models; df is the wave frequency bandwidth. The frequency components are uniformly distributed between the lower and upper cutoff frequencies, which are 0.1 f_{ce} and 0.5 f_{ce} respectively. The ith frequency component satisfies: $f_i = f_0 + i * \frac{(f_{uc}-f_{lc})}{2N_f}$ $(-N_f \le i \le N_f)$. Here, f_{uc} and f_{lc} are the upper and lower cutoff frequency, and N_f = 100. Each frequency component has a random initial phase. We perform our simulations using different bandwidths from 0.001 to 0.2 f_{ce} based on the observations (e.g., Gao et al., 2014), while keeping the wave power the same for all the models with different bandwidths. Amplitudes (B_w) of the simulated waves range from 10 pT to 1.5 nT based on the satellite observations (e.g., Cattell et al., 2008; Li et al., 2009, 2011; Meredith et al., 2012). All waves are generated at the equator and propagate along the magnetic field line to higher magnetic latitudes up to 30° considering the fact that chorus wave power near the dawnside, where chorus waves mostly frequently occur, is mainly confined within 30° magnetic latitude (e.g., Agapitov et al., 2018; Meredith et al., 2012). To avoid step-like functions near the lower and upper cutoff latitudes, the B_w latitudinal distribution is assumed as

$$B_w = \begin{cases} B_{w0}\tanh(|\lambda|)\tanh(30-|\lambda|) & 0 \le |\lambda| \le 30 \\ 0 & |\lambda| \ge 30 \end{cases} \quad (1)$$

Here λ is the magnetic latitude in unit of degree, and B_{w0} is the magnetic wave amplitude. The wave normal angle is set to 0 for all wave models, since we focus on the dependence on bandwidth and amplitude and the most intense whistler-mode waves are observed to propagate along magnetic field lines (Agapitov et al., 2018; Li et al., 2016; Santolík et al., 2014).

2.2 Simulation Settings

The TP simulation method uses the full Lorenz equations of motion, as described in Gan et al. (2020b). In this study, we set the background electron density to be $5\ cm^{-3}$ at L = 6, and assume it to remain constant along the field line until $|\lambda|$= 30°, where chorus waves are assumed to be present. For a fixed wave frequency spectrum model, 360 electrons are released from the equator at each grid in the pitch angle-energy space, while their initial gyro-phases are uniformly distributed between 0° and 360°. The electrons move initially towards the higher latitudes in the northern hemisphere and are mirrored back to the equator where the simulation ends. Pitch angle diffusion coefficients are calculated based on the test particle simulation results, using the following equation:

$$D_{\alpha\alpha} = \frac{<(\Delta\alpha - <\Delta\alpha>)^2>}{2\tau}, \quad (2)$$

where $\Delta\alpha$ is the equatorial pitch angle variation, $<\Delta\alpha>$ is the averaged equatorial pitch angle variation, and τ is the electron half-bounce period. Only pitch angle diffusion coefficients are calculated in this simulation for simplicity. Advection coefficients are also calculated using the test particle simulation results to quantify the NL effects. Advection coefficients are defined as:

$$V = \frac{<\Delta\alpha>}{2\tau} \quad (3)$$

As is shown in Gan et al. (2020b), the advection rates due to phase trapping and phase bunching by monochromatic whistler-mode wave have different characteristics. Phase trapping is distinguished by sustained resonance, lasting on the order of at least one phase oscillation period. Phase trapping leads to large positive advection, while phase bunching leads to relatively smaller advection, which is negative in most cases. This suggests that it is more reasonable to discuss the different NL processes separately in the case of monochromatic waves. However, in the case of broadband waves, it is very difficult to define and separate the NL phase trapping and bunching processes, since the distinction is not as clear. Thus, only the total advection as shown in equation (3) is discussed in this paper.

We use the Full Diffusion Code (e.g., Ma et al., 2018) to calculate the bounce-averaged diffusion coefficients with the same wave models described in section 2.1, representing the electron diffusion effects based on QL theory (e.g., Lyons, 1974). The background parameters are also set to be the same as those in test particle simulations.

3. Diffusion Coefficients and Nonlinear Effects of Different Models

3.1 Diffusion and Advection Coefficients Distribution in Pitch Angle-Energy Space

In this section, electron pitch angle diffusion coefficients ($D_{\alpha\alpha}$) and advection coefficients (V) are calculated using TP simulations in the pitch angle-energy space. Figures 1a-d show the simulation results of electrons interacting with weak whistler-mode waves with an amplitude of 10 pT. Distributions of $D_{\alpha\alpha}$ and V for waves with the bandwidth of 0.001 and 0.2 f_{ce} are shown in Figures 1a-b and Figures 1c-d respectively, where f_{ce} is the electron gyrofrequency at the magnetic equator. Figures 1e-h show the simulation results using strong whistler-mode

waves with B_w = 300 pT, following the same format as that of Figures 1a-d. The results indicate that the distribution of $D_{\alpha\alpha}$ is significantly affected by both the wave amplitude and bandwidth. For small amplitude waves, Figures 1a-b show similar $D_{\alpha\alpha}$ distributions. For larger amplitudes, however, the $D_{\alpha\alpha}$ distribution varies significantly with different bandwidths. For small amplitude waves (Figures 1c-d), advection for the narrow and broad bandwidths is close to zero, indicating pure diffusion processes. For large amplitude waves (Figures 1g-h), significant positive advection, as large as $0.4\ s^{-1}$, occurs at very small pitch angles, for both narrowband and broadband models. This is equivalent to averaged electron pitch angle variation of $20°$ during a half-bounce period. Both models produce close to zero advection for intermediate pitch angles and energies. The advection distribution indicates that for strong waves, both narrowband and broadband, the motions of small pitch angle electrons cannot be generalized to diffusion processes and exhibit significant mono-directional transport. For intermediate pitch angles and energies, however, expected phase trapping and phase bunching apparently compensate each other to produce close to zero advection. The zero-advection region and the small pitch angle region show different characteristics, which are discussed in section 3.2.

3.2 Diffusion Coefficient Distributions in Amplitude-Bandwidth Space

As shown in Figures 1g-h, for intermediate pitch angle electrons with energy of several hundred keV, the advection is relatively small. Thus, we focus on the diffusion coefficient and quantify its dependence on wave amplitude and bandwidth. Waves with bandwidths of 0.001, 0.002, 0.004, 0.01, 0.1, 0.2 f_{ce} are used in the simulations, with amplitudes ranging from 10 to 1500 pT with a step of 10 pT. Two different cases are chosen in the electron pitch angle-energy space (Case 1: $\alpha = 40^{\circ}$ and E = 750 keV (Figures 2a-d); Case 2: $\alpha = 70^{\circ}$ and E = 450 keV (Figures 2e-h)), which are marked by the star and plus symbols in Figures 1g-h. To further help our analysis, we used the inhomogeneity ratio S (Omura et al., 2007), which is based on the monochromatic wave theory, as a reference for nonlinearity. Here S is defined as:

$$S = \frac{1}{\omega_t^2 \delta^2} \left\{ \left[\left(1 + \frac{\delta^2}{2} \frac{\Omega_e - \gamma\omega}{\Omega_e - \omega} \right) V_R - \frac{k\gamma v_\perp^2}{2\Omega_e} \right] \frac{\partial \Omega_e}{\partial h} \right\} \quad (4)$$

For all models including the broadband wave models, the wave frequency ω is set to the central frequency of 0.3 f_{ce}. Definition of the other parameters in equation (4) can be found in Omura et al. (2007). For B_w = 10 pT, Case 1 has the inhomogeneity ratio S of 6.416, and Case 2 has S of 1.648. Based on the theory of monochromatic waves, nonlinear interactions are expected to be more significant in Case 2 which has smaller inhomogeneity ratio. Distributions of $D_{\alpha\alpha}$ versus B_w are shown in Figure 2a, color coded for different bandwidths. Solid lines represent QL $D_{\alpha\alpha}$ for each case of non-monochromatic whistler-mode waves, and dashed lines are from the TP results. The dotted lines are also calculated with the TP simulations but using a monochromatic wave with the frequency of 0.3 f_{ce}. The ratio between the TP and QL simulation results is shown in Figure 2b using the same format. Monochromatic TP results are compared to the QL result simulated with bandwidth of 0.001 f_{ce}. As shown by Albert (2010), QL diffusion coefficients in the narrowband limit are the same as the monochromatic wave results in the quasilinear regime. In Figure 2c, the power index m of $D_{\alpha\alpha}$ for each model is calculated as:

$$m = \frac{d}{d log(B_w)} log(D_{\alpha\alpha}), \quad (5)$$

where B_w is the wave amplitude. In quasilinear theory, m equals to 2.

The diffusion coefficients and other related parameters described above are defined within the QL theory. Thus, although the disagreement between TP and QL diffusion coefficients provide some information of the nonlinear effects, it is still insufficient to quantify the nonlinear phase bunching and trapping. The diffusion (even if TP diffusion rates deviate from QL diffusion rates) and advection due to the phase bunching can be incorporated into the Fokker-Planck equation, because they describe the sufficiently slow change in electron distribution and can be modeled by differential operators. The phase trapping, however, is responsible for large pitch angle and energy changes for a single resonance. A phase trapping contribution to the electron distribution evolution cannot be described by the differential operators, and instead various forms of integral operators have been considered (e.g., Omura et al., 2015; Vainchtein et al., 2018). Therefore, it is important to quantify the wave parametric range in which the effects of large changes in pitch angle and energy (due to phase trapping) are negligible. As there is no good definition of the phase trapping for broadband waves, we define the "successive resonant acceleration" (SRA) regime that is characterized by pitch angle changes comparable to the changes due to the phase trapping in the system with the same wave amplitude and one frequency component (monochromatic wave). The pitch angle of the SRA electrons satisfies the following equation:

$$\Delta\alpha \geq \frac{2}{3}\Delta\alpha_{tr} \tag{6}$$

Here $\Delta\alpha$ is the equatorial pitch angle variation of the electrons during the simulation, and $\Delta\alpha_{tr}$ is the pitch angle variation expected from phase trapping calculated based on the monochromatic wave theory (Vainchtein et al., 2018). Moreover, we assume the electrons stay in resonance until they reach the equator when calculating $\Delta\alpha_{tr}$. For models using the narrowband waves, SRA electrons correspond to electrons that are accelerated through phase trapping, where the $\frac{2}{3}$ accounts for the detrapping caused by perturbations from non-resonant frequencies. For models with broadband waves, phase trapping processes are destroyed by the incoherent wave structures. Thus, SRA electrons are not phase trapped, but are significantly accelerated by multiple resonant scattering during the simulation. SRA electrons in the broadband models indicate that the diffusive acceleration is comparable to the NL expectations, which leads to non-quasilinear features, as discussed in the following sections. The ratio of the SRA electrons to the total electron number is shown in Figure 2d for Case 1 ($\alpha = 40^{\circ}$ and E = 750 keV), color coded for different non-monochromatic and monochromatic waves. Figures 2e-h show the results for Case 2 ($\alpha = 70^{\circ}$ and E = 450 keV) in the same format as Figures 2a-d.

For Case 1 ($\alpha = 40^{\circ}$ and E = 750 keV), TP $D_{\alpha\alpha}$ of the broadband models ($df \geq 0.01\, f_{ce}$) agree well with the QL results for all amplitudes (Figures 2a & 2b), with a constant m value of 2 (Figure 2c). The SRA ratio of the broadband models is close to 0 for all amplitudes, suggesting small nonlinear effects. For monochromatic models, TP $D_{\alpha\alpha}$ is consistent with the QL results for B_w < 100 pT, as shown in Figures 2a & 2b. Two 'bumps' (shaded regions) mark the larger $D_{\alpha\alpha}$ at intermediate amplitudes, with the first bump at 150-400 pT, and the second at 400-700 pT. Electron trajectories of the first and second bump are shown in Figures 4a & 4b correspondingly. Phase trapping and phase bunching result in a large spread in the electron pitch angle distributions, which then lead to larger $D_{\alpha\alpha}$. Monochromatic TP $D_{\alpha\alpha}$ drops to much smaller values compared to the QL results at very large amplitudes (>700 pT). The corresponding electron trajectories are shown in Figure 4c, where electron phase trapping is limited by the early detrapping. The limited phase trapping processes lead to the decrease of $D_{\alpha\alpha}$. Power index m of

monochromatic models equals to 2 at small amplitudes (< 100 pT), which is consistent with the QL theory (Figure 2c). The SRA ratio of the monochromatic model shows one significant bump corresponding to the second bump in $D_{\alpha\alpha}$ distribution (400-700 pT), which suggests the key role of NL phase trapping in the enhancement of $D_{\alpha\alpha}$ in the second bump. The SRA ratio drops to 0 at very large amplitudes, which results from the detrapping of electrons, as shown in Figure 4c. The detrapping also leads to the decrease of $D_{\alpha\alpha}$, as described earlier in Figure 2a. Results of the narrowband models ($df \leq 0.01\ f_{ce}$) follow a similar trend to that of the monochromatic model, and become more similar to the QL results as bandwidth increases. Note that the full electron trajectories at different B_w of Case 1 for monochromatic, narrowband, and broadband waves are shown in Figure S1 in the Supporting Information (SI), which confirms the nonlinear phase trapping/bunching, and diffusive scattering features discussed above.

For Case 2 ($\alpha = 70^{\circ}$ and E = 450 keV), TP $D_{\alpha\alpha}$ of the broadband models ($df \geq 0.01\ f_{ce}$) agrees with the QL results for B_w < 600 pT (Figures 2e & 2f). TP/QL ratio of broadband models drop below 1 to very small values for B_w > 600 pT, which is different from Case 1. The corresponding power index m deviates from 2 when B_w > 600 pT and drops to 0 gradually as B_w increases to 1500 pT (Figure 2g). The SRA ratios of the broadband models remain 0 for B_w ~ 10–300 pT. The SRA ratios increase significantly to 10% as B_w increases from 300 pT to 1500 pT, which leads to the decrease of TP/QL ratio, as described above. Such an SRA ratio increase is due to the modulation of electron scattering by the phase trapping trajectory, as shown in Figure 4f. The upper limit of electron scattering in TP simulation is limited by the resonant curve (dashed line), which is the electron resonant pitch angle/energy along a magnetic field line (Vainchtein et al., 2018), while QL simulation lacks such limit. This indicates that although broadband models produce diffusion processes at large amplitudes, standard bounce-averaged QL theory is inapplicable. The method of bounce-averaging diffusion coefficients along an unperturbed electron trajectory becomes invalid, as the wave amplitude is so strong that the electron pitch angles and energies are scattered significantly even within one quarter-bounce period. For monochromatic and broadband models, Case 2 results show similar distributions to those of Case 1, but with nonlinear features evident at smaller amplitudes. The two bumps in Case 2, which also resulted from NL phase trapping and bunching (Figures 4d & 4e), have the amplitude range of 50-200 pT instead of 150-700 pT in Case 1. $D_{\alpha\alpha}$ drops to small values at B_w > 200 pT, corresponding to the decrease of SRA ratio. The decrease is also due to electron detrapping, as shown in Figures S2c & S2f. As shown by both Case 1 and Case 2, for narrowband whistler-mode waves with the bandwidth smaller than 0.01 f_{ce}, NL effects lead to enhanced $D_{\alpha\alpha}$ at intermediate amplitudes. At very large amplitudes, TP $D_{\alpha\alpha}$ of these narrowband models are much smaller than the QL ones. For broadband models with bandwidth larger than 0.01 f_{ce}, TP $D_{\alpha\alpha}$ keeps consistent with QL results for most amplitude ranges. However, for Case 2 with relatively small inhomogeneity ratio, TP $D_{\alpha\alpha}$ becomes smaller than QL ones due to the increase of SRA electrons. Trajectories of these electrons exhibit diffusion characteristics, but the acceleration processes are limited by the resonant curve along the background field line.

3.3 Diffusion and Advection Coefficient Distributions in Amplitude-Bandwidth Space for Electrons with Small Pitch Angles

We discuss $D_{\alpha\alpha}$ and V distribution of small pitch angle regions separately. Case 3 with initial pitch angle of 5° and initial energy of 20 keV is shown in Figure 3 with the same format as Figure 2. For broadband models ($df \geq 0.01\ f_{ce}$), TP $D_{\alpha\alpha}$ stays consistent with the QL results at

B_w < 80 pT (Figure 3a), increases at slower rates for B_w > 80 pT, leading to TP/QL ratio much smaller than 1 (Figure 3b), and reaches a constant value for B_w > 600 pT. Advection V of the broadband models increases as amplitude increases for B_w > 30 pT, and reaches its maximum constant value at 1000 pT (Figure 3c). The large SRA ratio of the broadband models suggests that the upper limits of diffusion trajectories are modulated by anomalous phase trapping (solid line in Figure 4i), similar to those of Case 2 (Kitahara & Katoh, 2019). As the SRA ratio increases with increasing amplitude, V becomes saturated, when SRA ratio saturates at B_w ~ 1000 pT. These distributions indicate that SRA electrons of the broadband models play important roles in limiting $D_{\alpha\alpha}$ and V at very large amplitudes.

For monochromatic and narrowband models, TP $D_{\alpha\alpha}$ agrees with QL results for B_w < 80 pT (Figure 3a). A bump between 80 pT and 150 pT, as shown in Figures 3a & 3b, marks the larger TP $D_{\alpha\alpha}$ compared to the QL results. A plateau follows for B_w up to 250 pT, above which $D_{\alpha\alpha}$ decreases significantly to much smaller values. Advection V of the narrowband and monochromatic models also shows a bump at the same amplitude range (Figure 3c). For B_w > 150 pT, V increases at slower rates for B_w ~ 150–250 pT (plateau), and subsequently becomes saturated for B_w > 300 pT. The bumps and plateau result from anomalous trapping electrons, as shown in Figures 4g-h. The SRA ratios of monochromatic and narrowband models increase from 0 to 100%, for B_w ~ 80 –250 pT, corresponding to the bump and plateau. When the SRA ratio reaches 100% (> 300 pT), all electrons are anomalously trapped. The fully trapped electron population leads to maximum advection effects where all electrons are accelerated along the resonant curve (Figure 4h). On the other hand, phase trapping processes lead to close to zero scattering effects, resulting in the minimum $D_{\alpha\alpha}$, which is shown in Figure 4h. As shown by Case 3, broadband TP $D_{\alpha\alpha}$ deviates from standard QL values at much lower amplitudes compared to Case 1 and Case 2. This is probably due to the effect of very large SRA ratio, which also leads to strong advection at several hundred pT. For narrowband waves, strong anomalous trapping contributes to the enhanced $D_{\alpha\alpha}$ and V at intermediate amplitudes. The same process also results in the rapid decrease of $D_{\alpha\alpha}$ and saturation of V at larger amplitudes. Overall, non-quasilinear features are more significant for cases of small initial electron pitch angles compared to larger pitch angles.

4. Quasilinear and Diffusion Regimes

Applicability of QL theory in amplitude-bandwidth space is evaluated by comparing TP $D_{\alpha\alpha}$ to QL results. QL theory is set applicable if $D_{\alpha\alpha}$ of the two models satisfies:

$$0.5 < \frac{D_{\alpha\alpha}^{TP}}{D_{\alpha\alpha}^{QL}} < 2, \quad (7)$$

where $D_{\alpha\alpha}^{TP}$ ($D_{\alpha\alpha}^{QL}$) is the diffusion coefficient calculated from TP (QL) simulations. Multiple energies and pitch angles of electrons are tested, as shown in Figure 5a, with symbols (colors) representing different pitch angles (energies).

Figure 5b shows the QL regime evaluated using equation (7). The green region represents the amplitude and bandwidth where QL theory is applicable for all the cases selected in Figure 5a. Colored symbols represent the maximum amplitude of QL regime for each bandwidth, corresponding to the pitch angles and energies shown in Figure 5a. For narrowband models ($df < 0.01 f_{ce}$), the QL method is applicable for B_w ~20–50 pT. For broadband models ($df \geq 0.01 f_{ce}$), the maximum amplitude of the QL regime increases with increasing bandwidth from 50 pT ($df = 0.01\, f_{ce}$) to 300 pT ($df = 0.2\, f_{ce}$). The maximum amplitudes (where the QL theory is

valid) of four cases with the smallest inhomogeneity ratio S (calculated at 10 pT) are shown in Figure 5b. The maximum amplitudes increase significantly with increasing S at narrowband regions. The hidden colored symbols are all at larger amplitudes compared to the orange squares, and the full QL boundaries for all simulated electron energies and pitch angles are shown in Figure S3b. Gao et al. (2014) demonstrated that rising and falling tone chorus, as one of the most important whistler-mode waves, has the most probable bandwidth of 0.01 f_{ce}, and hiss-like chorus has the bandwidth of 0.025 f_{ce}. This indicates that at L-shell of 6, for rising/falling tone chorus (hiss-like emissions), QL theory is applicable for $B_w < 50$ pT ($B_w < 80$ pT), as inferred from Figure 5b.

As discussed above, the maximum QL amplitude is related to the inhomogeneity ratio S. To further analyze this correlation, we map the simulation results in the amplitude-bandwidth space (Figure 5b) to the inhomogeneity ratio-bandwidth (S-df) space (Figure 5c), where S is defined in equation (4). For any given grid in the S-df space, if all the simulation cases satisfy equation (7), all the cases are quasilinear, and then the grid is identified as the QL regime. If none of the simulation cases satisfy equation (7), the grid is identified as the NL regime. The region where part of the simulation cases satisfy equation (7) is categorized as the transition regime. As shown in Figure 5c, for narrowband whistler-mode waves ($df < 0.01\ f_{ce}$), The maximum wave amplitude for QL regime becomes larger as the bandwidth increases. More specifically, the QL regime expands as minimum S of QL regime decreases from 2.5 to 0.4, when bandwidth increases from 0.001 to 0.01 f_{ce}. Note that for monochromatic whistler-mode waves, the minimum S for QL regime is 1 (Omura et al., 2007). For broadband waves ($df < 0.01\ f_{ce}$), the minimum S for QL regime decreases slightly from 0.4 to 0.2, showing a smaller sensitivity to the wave bandwidth, compared to the narrowband region. The NL regime is distributed in small S regions, where the maximum S oscillates between 0.01 to 0.02 for bandwidth of 0.001 to 0.04 f_{ce}. For larger bandwidths, the maximum S decreases to 0.004. Figure 5c shows that most of the S and bandwidth ranges fall in the QL and transition regime.

Although QL theory is not applicable under some conditions, e.g., in the transition regime, the diffusion model may still be applicable. Two main nonlinear effects, phase trapping and phase bunching, produce particle transport with opposite $< \Delta\alpha >$ values, and for the long-term dynamics these two processes compensate each other (e.g., Artemyev et al., 2018). However, the net $< \Delta\alpha >$ can be nonzero, and although such $< \Delta\alpha >$ does not describe the electron distribution evolution (because even zero net $< \Delta\alpha >$ does not guarantee an absence of a strong acceleration due to trapping), the magnitude of $< \Delta\alpha >$ can serve as a measure of contribution of nonlinear resonances to the long-term electron distribution dynamics. If diffusion dominates over advection, the long-term evolution of the electron distribution function can still be generalized to diffusion processes, though it may not be quasilinear, i.e., the diffusion coefficients can differ from the QL model coefficients. Thus, it is critical to identify the diffusion regimes in the amplitude-bandwidth space to determine the conditions under which a modified Fokker-Planck equation is applicable. Using the TP simulation results, a diffusion regime satisfies the following criterion:

$$\frac{< \Delta\alpha >}{(< (\Delta\alpha - < \Delta\alpha >)^2 >)^{0.5}} < 1 \quad (8)$$

Here, $\Delta\alpha$ is the electron pitch angle variation, and $< \Delta\alpha >$ is the average electron equatorial pitch angle variation during the simulation. It is worth noting that advection accumulates linearly with time while diffusion accumulates with the square-root of time. The

contribution from diffusion processes decreases compared to advection when the timescale of interest increases. Thus, equation (8) is only applicable when discussing the timescale of a bounce-period. However, taking into account that the occurrence rate of intense whistler-mode waves, which are in many cases chorus waves nonlinearly resonating with electrons, is smaller than the wave occurrence rate with weak-to-modest amplitudes (e.g., Zhang et al., 2018), there are many diffusive interactions between rare nonlinear interactions. Therefore, the ratio from equation (8) suggests that diffusion would dominate the electron distribution function evolution on a time scale much longer than the bounce-period. This time scale would be even longer if we take into account that many intense chorus waves may not resonate nonlinearly with electrons due to the strong modulation and/or phase decoherence (Zhang et al., 2020, and references therein). The distribution of the diffusion regime during a bounce period is shown in Figure 5d. Similar to Figure 5b, the green regions represent amplitudes and bandwidths where equation (8) is satisfied for all cases. The maximum amplitude of diffusion regime for narrowband models increases from 60 pT to 400 pT as bandwidth increases from 0.001 f_{ce} to 0.01 f_{ce}. Broadband models (> 0.01 f_{ce}) have roughly a constant maximum amplitude between 300 pT and 400 pT. Interactions with small pitch angle electrons lead to much larger advection, compared to electrons with larger pitch angles, thus limiting the diffusion regimes. Therefore, we identify another diffusion regime, where small pitch angle electrons are excluded. This extends the original green regions to amplitudes up to 1500 pT for bandwidths from 0.01 to 0.05 f_{ce}, and the extended region is marked by grey areas in Figure 5d. Maximum diffusion amplitudes of the small pitch angle cases are marked by colored plus signs in Figure 5d. Note that green diffusion regime is significantly limited by the small pitch angle cases for broadband models (> 0.01 f_{ce}). The boundary of the diffusion regime without these cases is marked by the black dashed line, and the colored symbols represent the simulation cases determining the boundary, corresponding to symbols shown in Figure 5a. This boundary is mainly limited by the cases from the minimum resonant energies, which has the smallest inhomogeneity ratio values.

As discussed earlier, the diffusion regime narrows down when the timescale of interest increases. On the other hand, it is inappropriate to assume that electrons interact with the same wave and that advection can accumulate linearly for an infinite amount of time. For the same wave packet, it is reasonable to assume consistent advection which increases linearly with time, while the diffusion effect is proportional to the square-root of time. We then expand our diffusion regime analysis to the timescales of electron interaction with a typical chorus wave packet, considering the fact that chorus is one of the most commonly observed intense whistler-mode waves in the Earth's radiation belts. Electrons are assumed to drift across one chorus wave packet with a scale size of 300 km (Shen et al., 2019) within the total time of T_{drift}. The diffusion regime criterion of a bounce period, as shown in equation (8), can then be transformed to:

$$\frac{< \Delta\alpha > \frac{T_{drift}}{NT_{bounce}}}{\left(< (\Delta\alpha - < \Delta\alpha >)^2 > \frac{T_{drift}}{NT_{bounce}} \right)^{0.5}} < 1 \quad (9)$$

Here NT_{bounce} is the N bounce periods of electrons and number $N > 1$ corresponds to the cumulative effect of intense chorus occurrence rate ($N \sim$ 10-30, see Zhang et al., 2018) and chorus wave modulation (making N even larger, see Tao et al., 2013; Zhang et al., 2020); $\Delta\alpha$ and $< \Delta\alpha >$ are the same as those defined in equation (8). The distribution of diffusion regime for

the timescale of T_{drift} and $N = 1$ is shown in Figure 5e, with the same format as Figure 5d, and for $N = 30$ in Figure S4. Figure 5e shows the narrowest diffusion regimes defined by equation (9) with the maximum occurrence rate for NL waves, *i.e.,* waves that are intense enough for nonlinear processes. $N = 30$ may be more realistic considering all the subpacket structures within a chorus packet. Both green and grey diffusion regions are smaller in Figure 5e compared to Figure 5d. The boundary of green region is determined by the small pitch angle electrons with a maximum amplitude of ~50 pT for all bandwidths. The grey region, which is limited by the electrons near the minimum resonant energies, has a maximum amplitude of 50 to 100 pT for narrowband models ($df < 0.01f_{ce}$) and about 200 pT for broadband models ($df \geq 0.01f_{ce}$). For the most common chorus bandwidth of 0.01/0.025 f_{ce} (Gao et al., 2014), advection needs to be considered when $B_w > 200$ pT. Both Figures 5d and 5e present the importance of including advection terms when considering precipitation, since small electron pitch angles further limit the applicability of diffusion models.

5. Summary and Discussion

Using both TP and QL simulations, we quantitatively analyzed the distribution of electron pitch angle diffusion and advection coefficients in both pitch angle-energy space of electrons and amplitude-bandwidth space of whistler-mode waves. The corresponding advection distribution is also evaluated using TP simulations. We evaluated the applicability of quasilinear and diffusion models for a large range of electron pitch angles and energies, as well as whistler-mode wave amplitudes and bandwidths. The main findings of this study are summarized below.

1. Electron SRA by intense broadband whistler-mode waves is limited by phase trapping trajectory, which leads to smaller diffusion coefficients compared to QL results.
2. For narrowband whistler-mode waves, TP diffusion coefficients are larger than the QL results at intermediate amplitudes due to dominant nonlinear phase trapping and bunching, but are much smaller than the QL results at very large amplitudes.
3. Significant anomalous trapping occurs when small pitch angle electrons interact with intense narrowband whistler-mode waves (>100 pT), while significant SRA occurs when interacting with intense broadband waves. Both processes lead to small constant diffusion coefficients at very large wave amplitudes.
4. QL theory is applicable for narrowband waves ($df < 0.01f_{ce}$) for $B_w < 50$ pT, while for broadband waves ($df \geq 0.01f_{ce}$) it is applicable for $B_w < 300$ pT. This means that QL theory is still valid for rising/falling tone chorus ($df \sim 0.01\, f_{ce}$) with $B_w < 50$ pT, and hiss-like chorus ($df \sim 0.025\, f_{ce}$) with $B_w < 80$ pT.
5. Maximum amplitudes of diffusion regimes range from 50 pT for narrowband waves with $df < 0.01f_{ce}$ to 200 pT for broadband waves with $df \geq 0.01f_{ce}$, when the electron pitch angle is not too small. Diffusion regime of the small pitch angle electrons is significantly limited, and advection terms need to be added when small pitch angle electrons interact with whistler-mode waves with $B_w > 50$ pT.

Nonlinear effects are affected by the inhomogeneity ratio, as shown by the present study and many previous studies (e.g., Omura et al., 2007; Shklyar & Matsumoto, 2009; Tao & Bortnik, 2010). The threshold amplitude provided in this study varies significantly when the L-shell value changes, since S is roughly proportional to $(dB_0/dz)/B_w$, where B_w is the wave amplitude and B_0 is the background magnetic field strength. If we assume a dipole magnetic field model, the threshold amplitude is roughly $\left(\frac{L}{6}\right)^{-4}$ times the results in the present study since

our simulation is performed at $L \sim 6$ (under assumption of the same occurrence rate of intense whistler-mode waves for all L-shells, see details in Zhang et al., 2018). With these normalizations, our study provides valuable information for the application of QL theory in the modeling of radiation belt electron dynamics. We show that QL theory is applicable for whistler-mode waves with a wide range of bandwidths and amplitudes. However, it is also shown that for large amplitude whistler-mode waves, whether broadband or narrowband, quasilinear diffusion coefficients are inaccurate, and the diffusion model may not be applicable. Especially for electrons with small pitch angles, which are closely related to the energetic electron precipitation, advection needs to be considered and incorporated into the long-term models.

Acknowledgements and Data

This research at Boston University is supported by the NASA grants 80NSSC20K0698, 80NSSC19K0845 and 80NSSC20K0196, NSF grant AGS-1847818, and the Alfred P. Sloan Research Fellowship FG-2018-10936. LG gratefully acknowledges the NASA FINESST grant 80NSSC20K1506. A.V.A. acknowledges the NASA grant 80NSSC20K1578.

Open Research

The data used to produce figures in the manuscript are publicly available online (doi.org/10.6084/m9.figshare.16847815).

References

Agapitov, O. V., Artemyev, A. V., Mourenas, D., Krasnoselskikh, V., Bonnell, J., Contel, O. L., et al. (2014). The quasi-electrostatic mode of chorus waves and electron nonlinear acceleration. *Journal of Geophysical Research: Space Physics*, *119*(3), 1606–1626. https://doi.org/10.1002/2013JA019223

Agapitov, O. V., Artemyev, A. V., Mourenas, D., Mozer, F. S., & Krasnoselskikh, V. (2015). Nonlinear local parallel acceleration of electrons through Landau trapping by oblique whistler mode waves in the outer radiation belt. *Geophysical Research Letters*, *42*(23), 10,140-10,149. https://doi.org/10.1002/2015GL066887

Agapitov, O. V., Mourenas, D., Artemyev, A. V., Mozer, F. S., Hospodarsky, G., Bonnell, J., & Krasnoselskikh, V. (2018). Synthetic Empirical Chorus Wave Model From Combined Van Allen Probes and Cluster Statistics. *Journal of Geophysical Research: Space Physics*, *123*(1), 297–314. https://doi.org/10.1002/2017JA024843

Albert, J. M. (2000). Gyroresonant interactions of radiation belt particles with a monochromatic electromagnetic wave. *Journal of Geophysical Research: Space Physics*, *105*(A9), 21191–21209. https://doi.org/10.1029/2000JA000008

Albert, J. M. (2010). Diffusion by one wave and by many waves. *Journal of Geophysical Research: Space Physics*, *115*(A3). https://doi.org/10.1029/2009JA014732

Albert, J. M., Artemyev, A. V., Li, W., Gan, L., & Ma, Q. (2021). Models of Resonant Wave-Particle Interactions. *Journal of Geophysical Research: Space Physics*, *126*(6), e2021JA029216. https://doi.org/10.1029/2021JA029216

Albert, Jay M., Meredith, N. P., & Horne, R. B. (2009). Three-dimensional diffusion simulation of outer radiation belt electrons during the 9 October 1990 magnetic storm. *Journal of Geophysical Research: Space Physics*, *114*(A9). https://doi.org/10.1029/2009JA014336

Allanson, O., Watt, C. E. J., Ratcliffe, H., Allison, H. J., Meredith, N. P., Bentley, S. N., et al. (2020). Particle-in-Cell Experiments Examine Electron Diffusion by Whistler-Mode Waves: 2. Quasi-Linear and Nonlinear Dynamics. *Journal of Geophysical Research: Space Physics*, *125*(7), e2020JA027949. https://doi.org/10.1029/2020JA027949

An, Z., Wu, Y., & Tao, X. (2022). Electron Dynamics in a Chorus Wave Field Generated From Particle-In-Cell Simulations. *Geophysical Research Letters*, *49*(3), e2022GL097778. https://doi.org/10.1029/2022GL097778

Artemyev, A. V., Neishtadt, A. I., Albert, J. M., Gan, L., Li, W., & Ma, Q. (2021). Theoretical model of the nonlinear resonant interaction of whistler-mode waves and field-aligned electrons. *Physics of Plasmas*, *28*(5), 052902. https://doi.org/10.1063/5.0046635

Bell, T. F. (1984). The nonlinear gyroresonance interaction between energetic electrons and coherent VLF waves propagating at an arbitrary angle with respect to the Earth's magnetic field. *Journal of Geophysical Research: Space Physics*, *89*(A2), 905–918. https://doi.org/10.1029/JA089iA02p00905

Bellan, P. M. (2013). Pitch angle scattering of an energetic magnetized particle by a circularly polarized electromagnetic wave. *Physics of Plasmas*, *20*(4), 042117. https://doi.org/10.1063/1.4801055

Bortnik, J., Thorne, R. M., & Inan, U. S. (2008). Nonlinear interaction of energetic electrons with large amplitude chorus. *Geophysical Research Letters*, *35*(21). https://doi.org/10.1029/2008GL035500

Breneman, A. W., Crew, A., Sample, J., Klumpar, D., Johnson, A., Agapitov, O., et al. (2017). Observations Directly Linking Relativistic Electron Microbursts to Whistler Mode

Chorus: Van Allen Probes and FIREBIRD II. *Geophysical Research Letters*, *44*(22), 11,265-11,272. https://doi.org/10.1002/2017GL075001

Burtis, W. J., & Helliwell, R. A. (1969). Banded chorus—A new type of VLF radiation observed in the magnetosphere by OGO 1 and OGO 3. *Journal of Geophysical Research (1896-1977)*, *74*(11), 3002–3010. https://doi.org/10.1029/JA074i011p03002

Burton, R. K., & Holzer, R. E. (1974). The origin and propagation of chorus in the outer magnetosphere. *Journal of Geophysical Research (1896-1977)*, *79*(7), 1014–1023. https://doi.org/10.1029/JA079i007p01014

Cattell, C., Wygant, J. R., Goetz, K., Kersten, K., Kellogg, P. J., Rosenvinge, T. von, et al. (2008). Discovery of very large amplitude whistler-mode waves in Earth's radiation belts. *Geophysical Research Letters*, *35*(1). https://doi.org/10.1029/2007GL032009

Crabtree, C., Tejero, E., Ganguli, G., Hospodarsky, G. B., & Kletzing, C. A. (2017). Bayesian spectral analysis of chorus subelements from the Van Allen Probes. *Journal of Geophysical Research: Space Physics*, *122*(6), 6088–6106. https://doi.org/10.1002/2016JA023547

Cully, C. M., Bonnell, J. W., & Ergun, R. E. (2008). THEMIS observations of long-lived regions of large-amplitude whistler waves in the inner magnetosphere. *grl*, *35*(17), L17S16. https://doi.org/10.1029/2008GL033643

Demekhov, A. G., Trakhtengerts, V. Yu., Rycroft, M. J., & Nunn, D. (2006). Electron acceleration in the magnetosphere by whistler-mode waves of varying frequency. *Geomagnetism and Aeronomy*, *46*(6), 711–716. https://doi.org/10.1134/S0016793206060053

Demekhov, A. G., Trakhtengerts, V. Yu., Rycroft, M., & Nunn, D. (2009). Efficiency of electron acceleration in the Earth's magnetosphere by whistler mode waves. *Geomagnetism and Aeronomy*, *49*(1), 24–29. https://doi.org/10.1134/S0016793209010034

Drozdov, A. Y., Shprits, Y. Y., Orlova, K. G., Kellerman, A. C., Subbotin, D. A., Baker, D. N., et al. (2015). Energetic, relativistic, and ultrarelativistic electrons: Comparison of long-term VERB code simulations with Van Allen Probes measurements. *Journal of Geophysical Research: Space Physics*, *120*(5), 3574–3587. https://doi.org/10.1002/2014JA020637

Gan, L., Li, W., Ma, Q., Albert, J. M., Artemyev, A. V., & Bortnik, J. (2020). Nonlinear Interactions Between Radiation Belt Electrons and Chorus Waves: Dependence on Wave Amplitude Modulation. *Geophysical Research Letters*, *47*(4), e2019GL085987. https://doi.org/10.1029/2019GL085987

Gan, L., Li, W., Ma, Q., Artemyev, A. V., & Albert, J. M. (2020). Unraveling the Formation Mechanism for the Bursts of Electron Butterfly Distributions: Test Particle and Quasilinear Simulations. *Geophysical Research Letters*, *47*(21), e2020GL090749. https://doi.org/10.1029/2020GL090749

Gao, X., Li, W., Thorne, R. M., Bortnik, J., Angelopoulos, V., Lu, Q., et al. (2014). Statistical results describing the bandwidth and coherence coefficient of whistler mode waves using THEMIS waveform data. *Journal of Geophysical Research: Space Physics*, *119*(11), 8992–9003. https://doi.org/10.1002/2014JA020158

Glauert, S. A., Horne, R. B., & Meredith, N. P. (2014). Three-dimensional electron radiation belt simulations using the BAS Radiation Belt Model with new diffusion models for chorus, plasmaspheric hiss, and lightning-generated whistlers. *Journal of Geophysical Research: Space Physics*, *119*(1), 268–289. https://doi.org/10.1002/2013JA019281

578 Hikishima, M., Omura, Y., & Summers, D. (2010). Microburst precipitation of energetic
579 electrons associated with chorus wave generation. *Geophysical Research Letters*, *37*(7).
580 https://doi.org/10.1029/2010GL042678
581 Horne, R. B., Thorne, R. M., Glauert, S. A., Albert, J. M., Meredith, N. P., & Anderson, R. R.
582 (2005). Timescale for radiation belt electron acceleration by whistler mode chorus waves.
583 *Journal of Geophysical Research: Space Physics*, *110*(A3).
584 https://doi.org/10.1029/2004JA010811
585 Hsieh, Y.-K., & Omura, Y. (2017). Nonlinear dynamics of electrons interacting with oblique
586 whistler mode chorus in the magnetosphere. *Journal of Geophysical Research: Space*
587 *Physics*, *122*(1), 675–694. https://doi.org/10.1002/2016JA023255
588 Inan, U. S., Bell, T. F., & Helliwell, R. A. (1978). Nonlinear pitch angle scattering of energetic
589 electrons by coherent VLF waves in the magnetosphere. *Journal of Geophysical*
590 *Research: Space Physics*, *83*(A7), 3235–3253. https://doi.org/10.1029/JA083iA07p03235
591 Karpman, V. I. (1974). Nonlinear effects in the ELF waves propagating along the magnetic field
592 in the magnetosphere. *Space Science Reviews*, *16*(3), 361–388.
593 https://doi.org/10.1007/BF00171564
594 Karpman, V. I., Istomin, J. N., & Shklyar, D. R. (1975). Effects of Nonlinear Interaction of
595 Monochromatic Waves with Resonant Particles in the Inhomogeneous Plasma. *Physica*
596 *Scripta*, *11*(5), 278–284. https://doi.org/10.1088/0031-8949/11/5/008
597 Katoh, Y., Omura, Y., & Summers, D. (2008). Rapid energization of radiation belt electrons by
598 nonlinear wave trapping. *Annales Geophysicae*, *26*, 3451–3456.
599 https://doi.org/10.5194/angeo-26-3451-2008
600 Katoh, Yuto, & Omura, Y. (2004). Acceleration of relativistic electrons due to resonant
601 scattering by whistler mode waves generated by temperature anisotropy in the inner
602 magnetosphere. *Journal of Geophysical Research (Space Physics)*, *109*, A12214.
603 https://doi.org/10.1029/2004JA010654
604 Kennel, C. F., & Engelmann, F. (1966). Velocity Space Diffusion from Weak Plasma
605 Turbulence in a Magnetic Field. *The Physics of Fluids*, *9*(12), 2377–2388.
606 https://doi.org/10.1063/1.1761629
607 Kitahara, M., & Katoh, Y. (2019). Anomalous Trapping of Low Pitch Angle Electrons by
608 Coherent Whistler Mode Waves. *Journal of Geophysical Research: Space Physics*,
609 *124*(7), 5568–5583. https://doi.org/10.1029/2019JA026493
610 Le Queau, D., & Roux, A. (1987). Quasi-Monochromatic Wave Particle Interactions in
611 Magnetospheric Plasmas. *Solar Physics*, *111*, 59–80.
612 https://doi.org/10.1007/BF00145441
613 Li, W., Thorne, R. M., Angelopoulos, V., Bortnik, J., Cully, C. M., Ni, B., et al. (2009). Global
614 distribution of whistler-mode chorus waves observed on the THEMIS spacecraft.
615 *Geophysical Research Letters*, *36*(9). https://doi.org/10.1029/2009GL037595
616 Li, W., Bortnik, J., Thorne, R. M., & Angelopoulos, V. (2011). Global distribution of wave
617 amplitudes and wave normal angles of chorus waves using THEMIS wave observations.
618 *Journal of Geophysical Research: Space Physics*, *116*(A12).
619 https://doi.org/10.1029/2011JA017035
620 Li, W., Thorne, R. M., Bortnik, J., Tao, X., & Angelopoulos, V. (2012). Characteristics of hiss-
621 like and discrete whistler-mode emissions. *grl*, *39*(18), L18106.
622 https://doi.org/10.1029/2012GL053206

Li, W., Thorne, R. M., Ma, Q., Ni, B., Bortnik, J., Baker, D. N., et al. (2014). Radiation belt electron acceleration by chorus waves during the 17 March 2013 storm. *Journal of Geophysical Research: Space Physics*, *119*(6), 4681–4693. https://doi.org/10.1002/2014JA019945

Li, W., Santolik, O., Bortnik, J., Thorne, R. M., Kletzing, C. A., Kurth, W. S., & Hospodarsky, G. B. (2016). New chorus wave properties near the equator from Van Allen Probes wave observations. *Geophysical Research Letters*, *43*(10), 4725–4735. https://doi.org/10.1002/2016GL068780

Lyons, L. R. (1974). Pitch angle and energy diffusion coefficients from resonant interactions with ion–cyclotron and whistler waves. *Journal of Plasma Physics*, *12*(3), 417–432. https://doi.org/10.1017/S002237780002537X

Lyons, L. R., Thorne, R. M., & Kennel, C. F. (1972). Pitch-angle diffusion of radiation belt electrons within the plasmasphere. *Journal of Geophysical Research*, *77*(19), 3455–3474. https://doi.org/10.1029/JA077i019p03455@10.1002/(ISSN)2169-9402.RADBELTS

Ma, Q., Li, W., Bortnik, J., Thorne, R. M., Chu, X., Ozeke, L. G., et al. (2018). Quantitative Evaluation of Radial Diffusion and Local Acceleration Processes During GEM Challenge Events. *Journal of Geophysical Research: Space Physics*, *123*(3), 1938–1952. https://doi.org/10.1002/2017JA025114

Meredith, N. P., Horne, R. B., Sicard-Piet, A., Boscher, D., Yearby, K. H., Li, W., & Thorne, R. M. (2012). Global model of lower band and upper band chorus from multiple satellite observations. *Journal of Geophysical Research: Space Physics*, *117*(A10). https://doi.org/10.1029/2012JA017978

Mourenas, D., Zhang, X.-J., Artemyev, A. V., Angelopoulos, V., Thorne, R. M., Bortnik, J., et al. (2018). Electron Nonlinear Resonant Interaction With Short and Intense Parallel Chorus Wave Packets. *Journal of Geophysical Research: Space Physics*, *123*(6), 4979–4999. https://doi.org/10.1029/2018JA025417

Nunn, D., & Omura, Y. (2015). A computational and theoretical investigation of nonlinear wave-particle interactions in oblique whistlers. *Journal of Geophysical Research (Space Physics)*, *120*(4), 2890–2911. https://doi.org/10.1002/2014JA020898

O'Brien, T. P., Looper, M. D., & Blake, J. B. (2004). Quantification of relativistic electron microburst losses during the GEM storms. *Geophysical Research Letters*, *31*(4). https://doi.org/10.1029/2003GL018621

Omura, Y., Furuya, N., & Summers, D. (2007). Relativistic turning acceleration of resonant electrons by coherent whistler mode waves in a dipole magnetic field. *Journal of Geophysical Research: Space Physics*, *112*(A6). https://doi.org/10.1029/2006JA012243

Omura, Y., Miyashita, Y., Yoshikawa, M., Summers, D., Hikishima, M., Ebihara, Y., & Kubota, Y. (2015). Formation process of relativistic electron flux through interaction with chorus emissions in the Earth's inner magnetosphere. *Journal of Geophysical Research: Space Physics*, *120*(11), 9545–9562. https://doi.org/10.1002/2015JA021563

Santolík, O., Gurnett, D. A., Pickett, J. S., Parrot, M., & Cornilleau-Wehrlin, N. (2003). Spatio-temporal structure of storm-time chorus. *Journal of Geophysical Research: Space Physics*, *108*(A7). https://doi.org/10.1029/2002JA009791

Santolík, Ondřej, Macúšová, E., Kolmašová, I., Cornilleau-Wehrlin, N., & Conchy, Y. de. (2014). Propagation of lower-band whistler-mode waves in the outer Van Allen belt: Systematic analysis of 11 years of multi-component data from the Cluster spacecraft. *Geophysical Research Letters*, *41*(8), 2729–2737. https://doi.org/10.1002/2014GL059815

669 Schulz, M., & Lanzerotti, L. J. (2012). *Particle Diffusion in the Radiation Belts*. Springer
670 Science & Business Media.
671 Schulz, Michael, & Lanzerotti, L. J. (1974). Pitch-Angle Diffusion. In Michael Schulz & L. J.
672 Lanzerotti (Eds.), *Particle Diffusion in the Radiation Belts* (pp. 46–80). Berlin,
673 Heidelberg: Springer. https://doi.org/10.1007/978-3-642-65675-0_3
674 Shen, X.-C., Li, W., Ma, Q., Agapitov, O., & Nishimura, Y. (2019). Statistical Analysis of
675 Transverse Size of Lower Band Chorus Waves Using Simultaneous Multisatellite
676 Observations. *grl*, *46*(11), 5725–5734. https://doi.org/10.1029/2019GL083118
677 Shklyar, D., & Matsumoto, H. (2009). Oblique Whistler-Mode Waves in the Inhomogeneous
678 Magnetospheric Plasma: Resonant Interactions with Energetic Charged Particles. *Surveys*
679 *in Geophysics*, *30*(2), 55–104. https://doi.org/10.1007/s10712-009-9061-7
680 Shprits, Y. Y., Subbotin, D., & Ni, B. (2009). Evolution of electron fluxes in the outer radiation
681 belt computed with the VERB code. *Journal of Geophysical Research: Space Physics*,
682 *114*(A11). https://doi.org/10.1029/2008JA013784
683 Shumko, M., Turner, D. L., O'Brien, T. P., Claudepierre, S. G., Sample, J., Hartley, D. P., et al.
684 (2018). Evidence of Microbursts Observed Near the Equatorial Plane in the Outer Van
685 Allen Radiation Belt. *Geophysical Research Letters*, *45*(16), 8044–8053.
686 https://doi.org/10.1029/2018GL078451
687 Summers, D., & Omura, Y. (2007). Ultra-relativistic acceleration of electrons in planetary
688 magnetospheres. *Geophysical Research Letters*, *34*(24).
689 https://doi.org/10.1029/2007GL032226
690 Tao, X., & Bortnik, J. (2010). Nonlinear interactions between relativistic radiation belt electrons
691 and oblique whistler mode waves. *Nonlinear Processes in Geophysics*, *17*(5), 599–604.
692 https://doi.org/10.5194/npg-17-599-2010
693 Tao, X., Bortnik, J., Albert, J. M., Thorne, R. M., & Li, W. (2013). The importance of amplitude
694 modulation in nonlinear interactions between electrons and large amplitude whistler
695 waves. *Journal of Atmospheric and Solar-Terrestrial Physics*, *99*, 67–72.
696 https://doi.org/10.1016/j.jastp.2012.05.012
697 Tao, Xin, Bortnik, J., Albert, J. M., & Thorne, R. M. (2012). Comparison of bounce-averaged
698 quasi-linear diffusion coefficients for parallel propagating whistler mode waves with test
699 particle simulations. *Journal of Geophysical Research (Space Physics)*, *117*(A10),
700 A10205. https://doi.org/10.1029/2012JA017931
701 Thorne, R. M., Li, W., Ni, B., Ma, Q., Bortnik, J., Chen, L., et al. (2013). Rapid local
702 acceleration of relativistic radiation-belt electrons by magnetospheric chorus. *Nature*,
703 *504*(7480), 411–414. https://doi.org/10.1038/nature12889
704
705 Tsurutani, B. T., Lakhina, G. S., & Verkhoglyadova, O. P. (2013). Energetic electron (>10 keV)
706 microburst precipitation, 5–15 s X-ray pulsations, chorus, and wave-particle interactions:
707 A review. *Journal of Geophysical Research: Space Physics*, *118*(5), 2296–2312.
708 https://doi.org/10.1002/jgra.50264
709 Tyler, E., Breneman, A., Cattell, C., Wygant, J., Thaller, S., & Malaspina, D. (2019). Statistical
710 Occurrence and Distribution of High-Amplitude Whistler Mode Waves in the Outer
711 Radiation Belt. *Geophysical Research Letters*, *46*(5), 2328–2336.
712 https://doi.org/10.1029/2019GL082292
713 Vainchtein, D., Zhang, X.-J., Artemyev, A. V., Mourenas, D., Angelopoulos, V., & Thorne, R.
714 M. (2018). Evolution of Electron Distribution Driven by Nonlinear Resonances With

Intense Field-Aligned Chorus Waves. *Journal of Geophysical Research (Space Physics)*, *123*(10), 8149–8169. https://doi.org/10.1029/2018JA025654

Wilson, L. B., Cattell, C. A., Kellogg, P. J., Wygant, J. R., Goetz, K., Breneman, A., & Kersten, K. (2011). The properties of large amplitude whistler mode waves in the magnetosphere: Propagation and relationship with geomagnetic activity. *Geophysical Research Letters*, *38*(17). https://doi.org/10.1029/2011GL048671

Xiao, F., Su, Z., Zheng, H., & Wang, S. (2009). Modeling of outer radiation belt electrons by multidimensional diffusion process. *Journal of Geophysical Research: Space Physics*, *114*(A3). https://doi.org/10.1029/2008JA013580

Xiao, F., Su, Z., Zheng, H., & Wang, S. (2010). Three-dimensional simulations of outer radiation belt electron dynamics including cross-diffusion terms. *Journal of Geophysical Research: Space Physics*, *115*(A5). https://doi.org/10.1029/2009JA014541

Zhang, X. -J., Agapitov, O., Artemyev, A. V., Mourenas, D., Angelopoulos, V., Kurth, W. S., et al. (2020). Phase Decoherence Within Intense Chorus Wave Packets Constrains the Efficiency of Nonlinear Resonant Electron Acceleration. *Geophysical Research Letters*, *47*(20). https://doi.org/10.1029/2020GL089807

Zhang, X.-J., Thorne, R., Artemyev, A., Mourenas, D., Angelopoulos, V., Bortnik, J., et al. (2018). Properties of Intense Field-Aligned Lower-Band Chorus Waves: Implications for Nonlinear Wave-Particle Interactions. *Journal of Geophysical Research (Space Physics)*, *123*(7), 5379–5393. https://doi.org/10.1029/2018JA025390

Zhang, X.-J., Mourenas, D., Artemyev, A. V., Angelopoulos, V., Bortnik, J., Thorne, R. M., et al. (2019). Nonlinear Electron Interaction With Intense Chorus Waves: Statistics of Occurrence Rates. *grl*, *46*(13), 7182–7190. https://doi.org/10.1029/2019GL083833

Figures and Captions

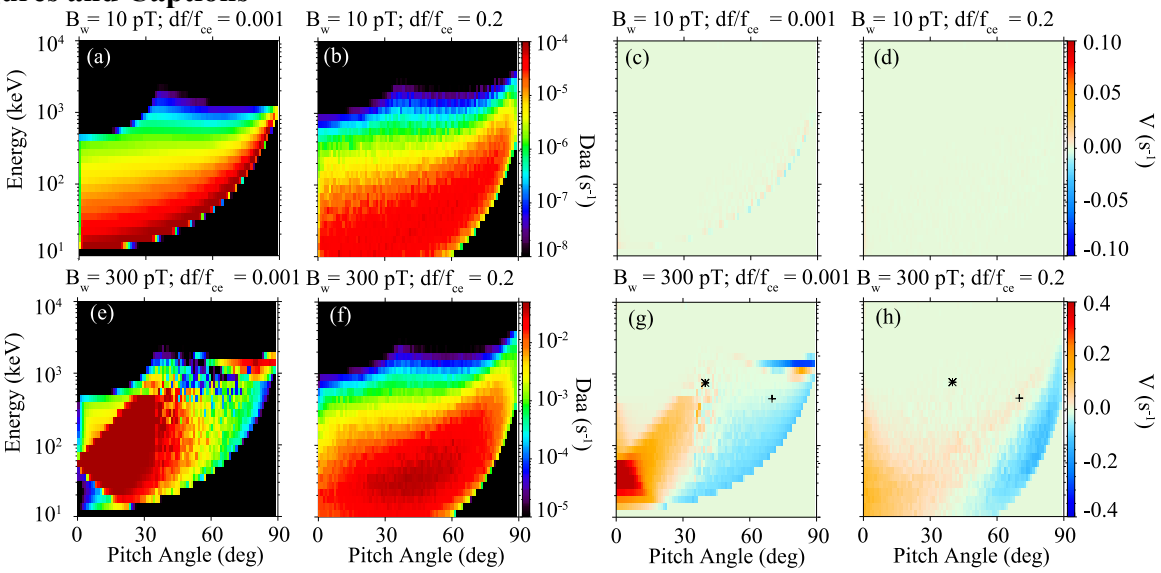

Figure 1. Diffusion and advection coefficients in pitch angle-energy space. (a) Diffusion coefficients calculated with the wave amplitude of 10 pT and bandwidth of 0.001 f_{ce}, and (b) the wave amplitude of 10 pT and bandwidth of 0.2 f_{ce}. (c) Advection coefficients calculated with the wave amplitude of 10 pT and bandwidth of 0.001 f_{ce} , and (d) the wave amplitude of 10 pT and the bandwidth of 0.2 f_{ce}. (e-h) Same as (a-d) but using the wave amplitude of 300 pT. The star and plus symbols in (g-h) represent the corresponding pitch angle and energy of Case 1 & 2 respectively.

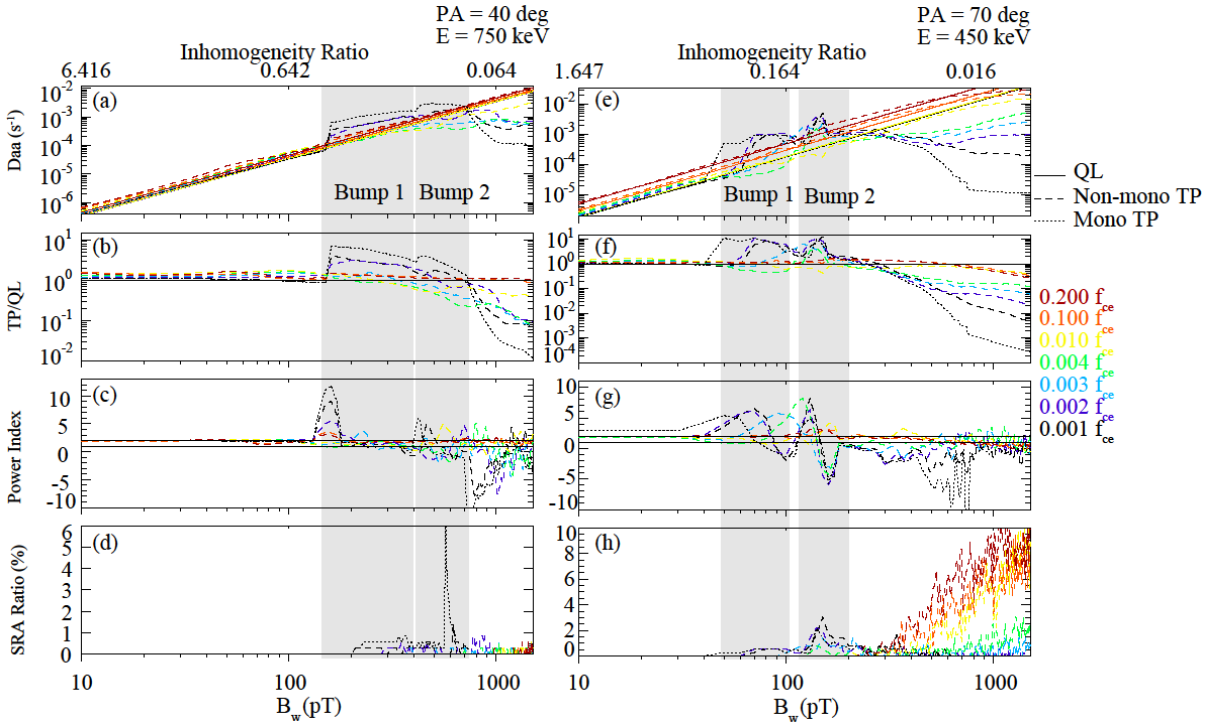

Figure 2. Diffusion coefficients analysis in amplitude-bandwidth space. (a) Diffusion coefficients for electrons with $\alpha = 40^{\circ}$ and $E = 750$ keV as a function of wave amplitude, color coded for different bandwidths. Solid lines are calculated using the quasilinear model, dashed lines are calculated using non-monochromatic test particle model, and the dotted line is calculated using monochromatic test particle model with the wave frequency of 0.3 f_{ce}. (b) The same format as (a) showing the ratio between diffusion coefficients calculated using test particle simulations and quasilinear ones; (c) power index of diffusion coefficients, and (d) SRA electron ratio. (e-h) The same format as (a-d) but showing the results for electrons with $\alpha = 70^{\circ}$ and $E =$ 450 keV.

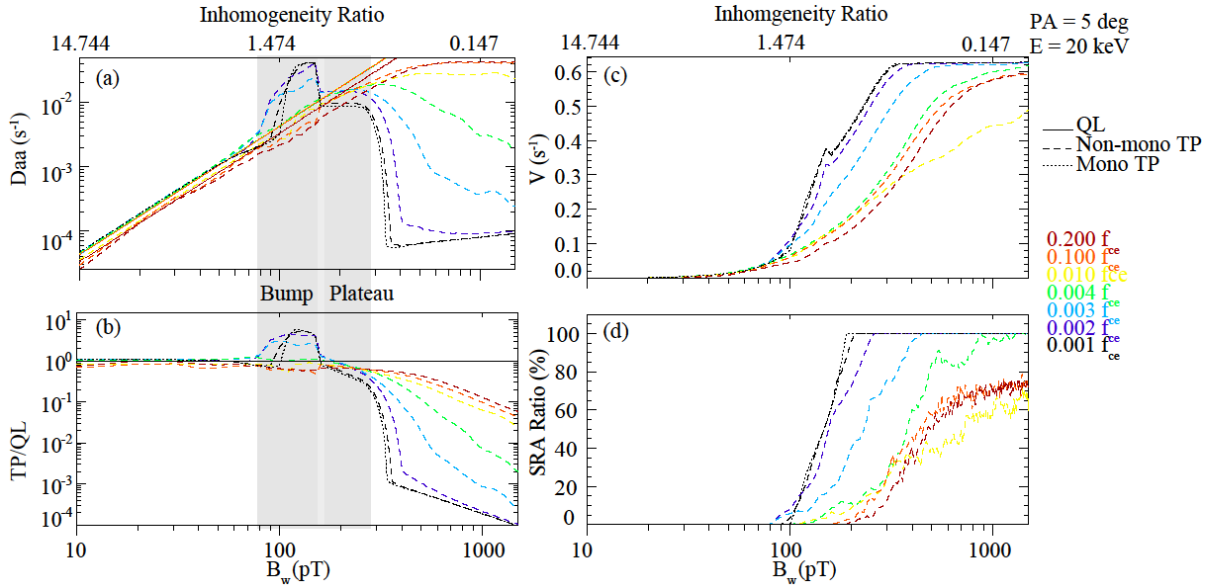

Figure 3. Diffusion and advection coefficients analysis for small pitch angle electrons with $\alpha = 5^{\circ}$ and $E = 20$ keV. (a) Diffusion coefficients as a function of whistler-mode wave amplitude, color coded for different bandwidths. Solid lines are calculated using the quasilinear model, dashed lines are calculated using test particle model, and the dotted line is calculated using monochromatic test particle model with the wave frequency of 0.3 f_{ce}. (b) The same format as (a), showing the ratio between the diffusion coefficients calculated using test particle simulations and quasilinear ones; (c) electron advection coefficients; and (d) SRA electron ratio.

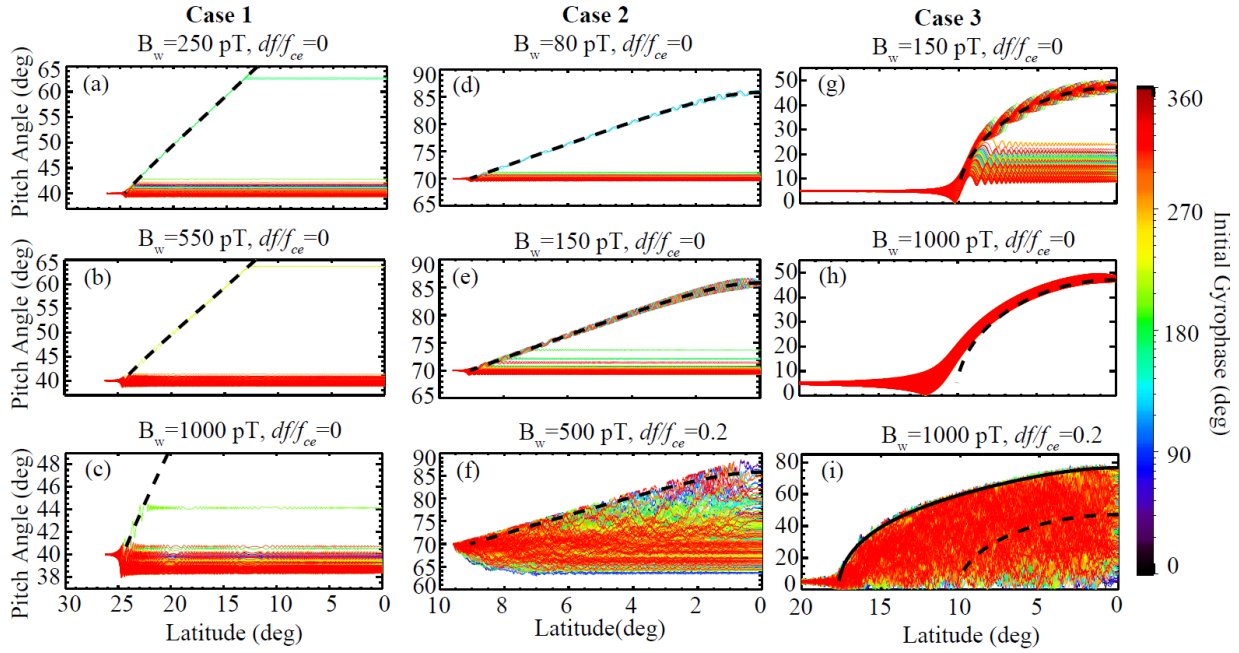

Figure 4. (a) Trajectories of Case 1 electrons interacting with monochromatic whistler-mode wave with the amplitude of 250 pT; (b) 550 pT; (c) 1000 pT. (d) Trajectories of Case 2 electrons interacting with monochromatic whistler-mode wave with the amplitude of 80 pT; (e) 150 pT; (f) whistler-mode wave with the amplitude of 500 pT and the bandwidth of 0.2 f_{ce}. (g) Trajectories of Case 3 electrons interacting with monochromatic whistler-mode wave with the amplitude of 150 pT; (e) 1000 pT; (f) whistler-mode wave with the amplitude of 1000 pT and the bandwidth of 0.2 f_{ce}. Black dashed lines are the electron phase trapping trajectories, calculated using the wave frequency of 0.3 f_{ce}, and the black solid line in Figure 4i is calculated using the frequency of 0.5 f_{ce}. Different colors represent different initial electron gyro-phases as shown in the colorbar.

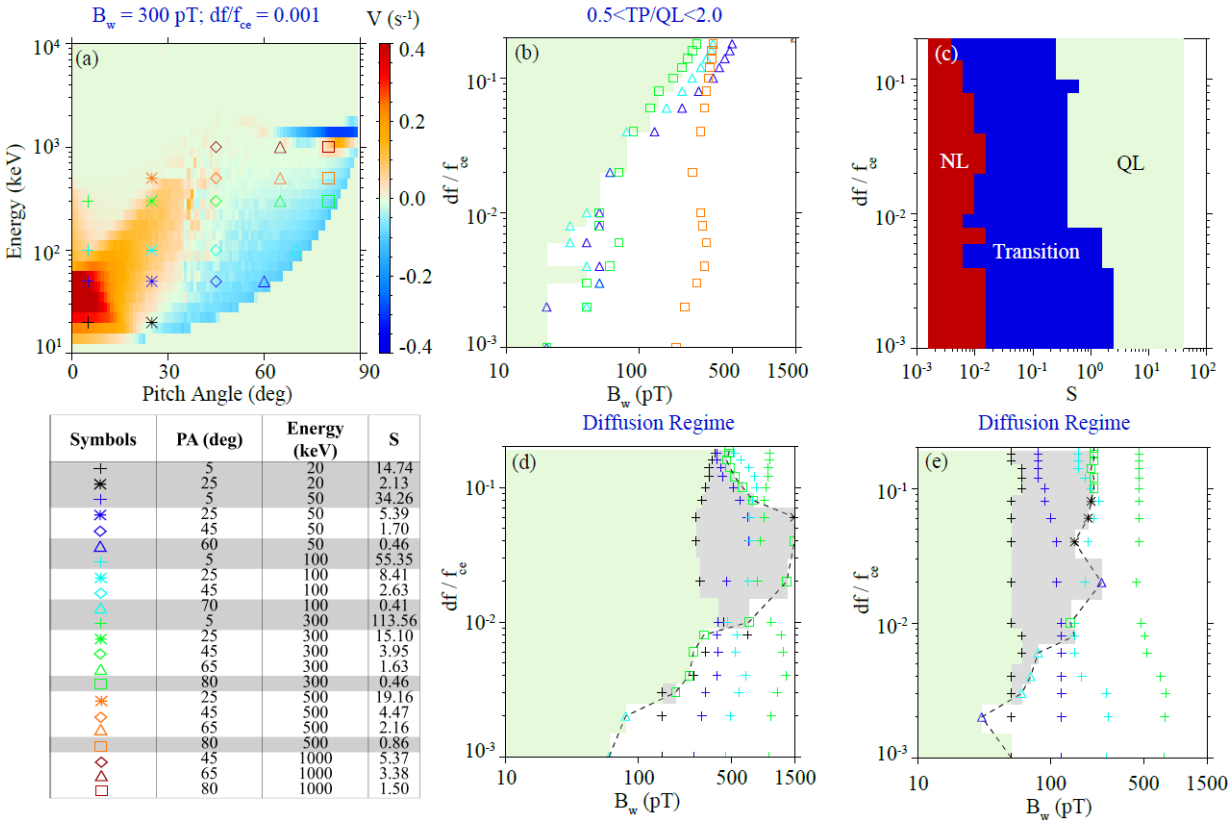

Symbols	PA (deg)	Energy (keV)	S
+	5	20	14.74
*	25	20	2.13
+	5	50	34.26
*	25	50	5.39
◇	45	50	1.70
△	60	50	0.46
+	5	100	55.35
*	25	100	8.41
◇	45	100	2.63
△	70	100	0.41
+	5	300	113.56
*	25	300	15.10
◇	45	300	3.95
△	65	300	1.63
□	80	300	0.46
*	25	500	19.16
◇	45	500	4.47
△	65	500	2.16
□	80	500	0.86
◇	45	1000	5.37
△	65	1000	3.38
□	80	1000	1.50

Figure 5. Distribution of quasilinear and diffusion regimes in amplitude-bandwidth space. (a) Distribution of simulated cases in pitch angle-energy space, where different colors (symbols) represent different energies (pitch angles), as labeled in the table. Only symbols of the shaded rows in the table are shown in (b-d) for simplicity. (b) Distribution of quasilinear regime (green) in amplitude-bandwidth space. Colored symbols represent the maximum wave amplitude of quasilinear regime at each bandwidth for the represented case. (c) Distribution of quasilinear (green), nonlinear (red), and transition (blue) regimes in inhomogeneity ratio-bandwidth space. (d) Same format as (b) showing diffusion regime distribution on the timescale of a bounce period, and (e) drifting time across a chorus wave packet (Shen et al., 2019). Grey regions in (d) & (e) are the extended diffusion regimes when excluding small pitch angle cases, and the dashed line marks the maximum wave amplitude of the grey region.

Figure1.

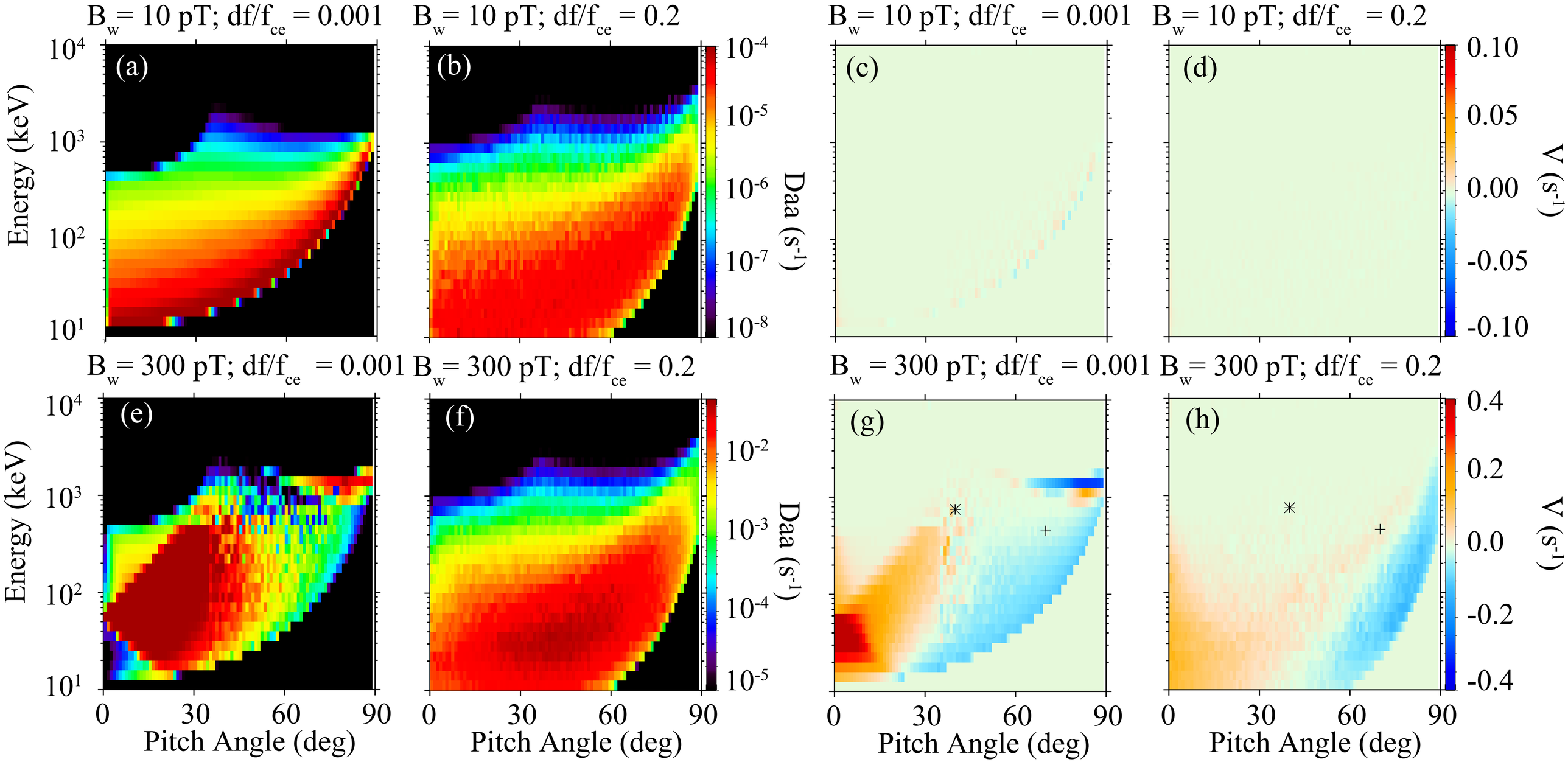
B_w = 10 pT; df/f_ce = 0.001
B_w = 10 pT; df/f_ce = 0.2
B_w = 10 pT; df/f_ce = 0.001
B_w = 10 pT; df/f_ce = 0.2
B_w = 300 pT; df/f_ce = 0.001
B_w = 300 pT; df/f_ce = 0.2
B_w = 300 pT; df/f_ce = 0.001
B_w = 300 pT; df/f_ce = 0.2
(a)
(b)
(c)
(d)
(e)
(f)
(g)
(h)
Energy (keV)
Pitch Angle (deg)
Daa (s^-1)
V (s^-1)

Figure2.

PA = 40 deg
E = 750 keV

PA = 70 deg
E = 450 keV

Inhomogeneity Ratio

6.416 0.642 0.064

1.647 0.164 0.016

(a) (b) (c) (d) (e) (f) (g) (h)

Bump 1 Bump 2

Daa (s^{-1})

TP/QL

Power Index

SRA Ratio (%)

B_w(pT)

QL
Non-mono TP
Mono TP

0.200 f_{ce}
0.100 f_{ce}
0.010 f_{ce}
0.004 f_{ce}
0.003 f_{ce}
0.002 f_{ce}
0.001 f_{ce}

Figure3.

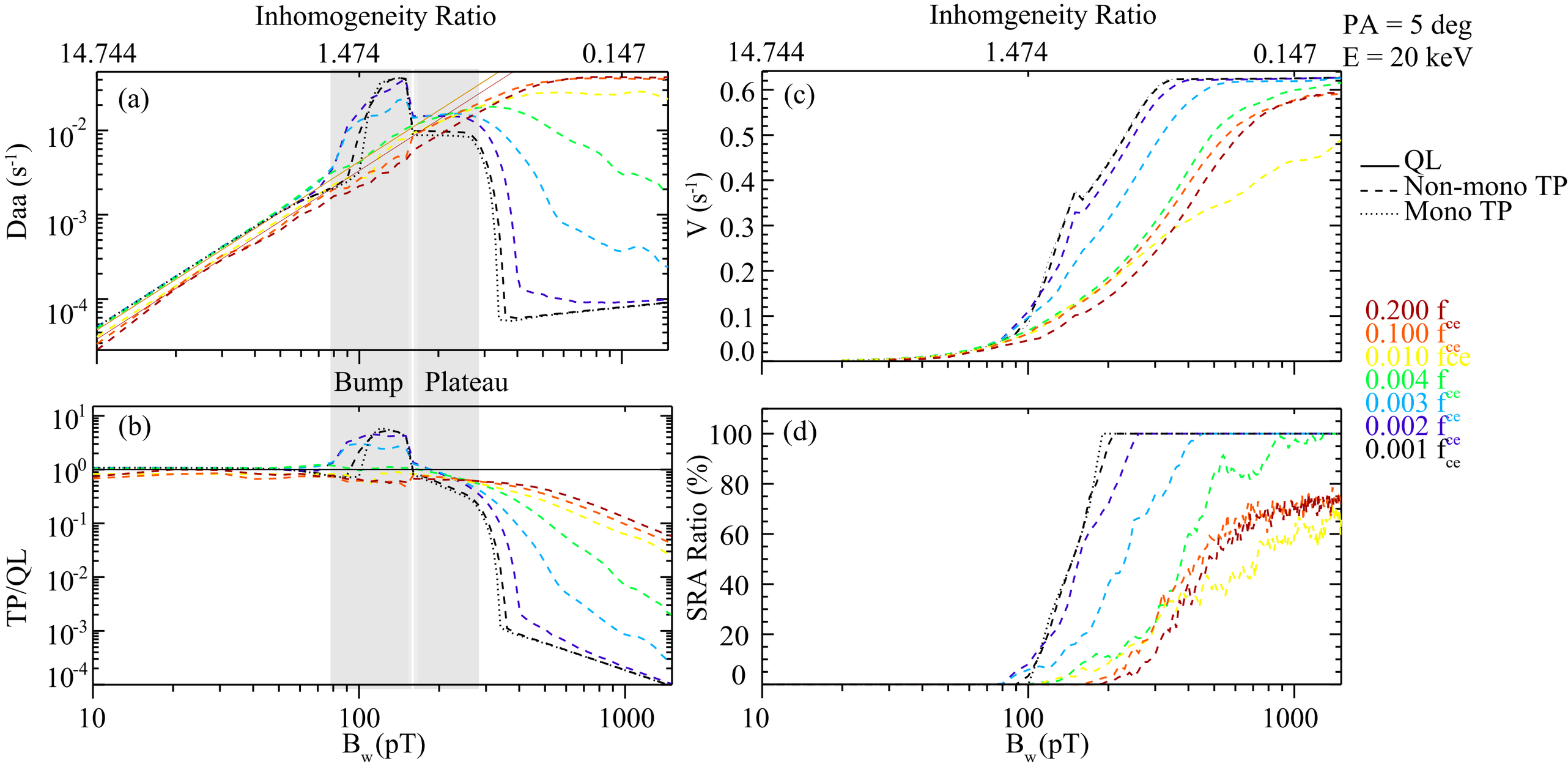
Inhomogeneity Ratio
14.744
1.474
0.147
(a)
Daa (s^{-1})
10^{-2}
10^{-3}
10^{-4}
Bump
Plateau
(b)
TP/QL
10^{1}
10^{0}
10^{-1}
10^{-2}
10^{-3}
10^{-4}
10
100
1000
B$_w$(pT)
Inhomgeneity Ratio
14.744
1.474
0.147
(c)
V (s^{-1})
0.6
0.5
0.4
0.3
0.2
0.1
0.0
(d)
SRA Ratio (%)
100
80
60
40
20
0
10
100
1000
B$_w$(pT)
PA = 5 deg
E = 20 keV
QL
Non-mono TP
Mono TP
0.200 f$_{ce}$
0.100 f$_{ce}$
0.010 f$_{ce}$
0.004 f$_{ce}$
0.003 f$_{ce}$
0.002 f$_{ce}$
0.001 f$_{ce}$

Figure4.

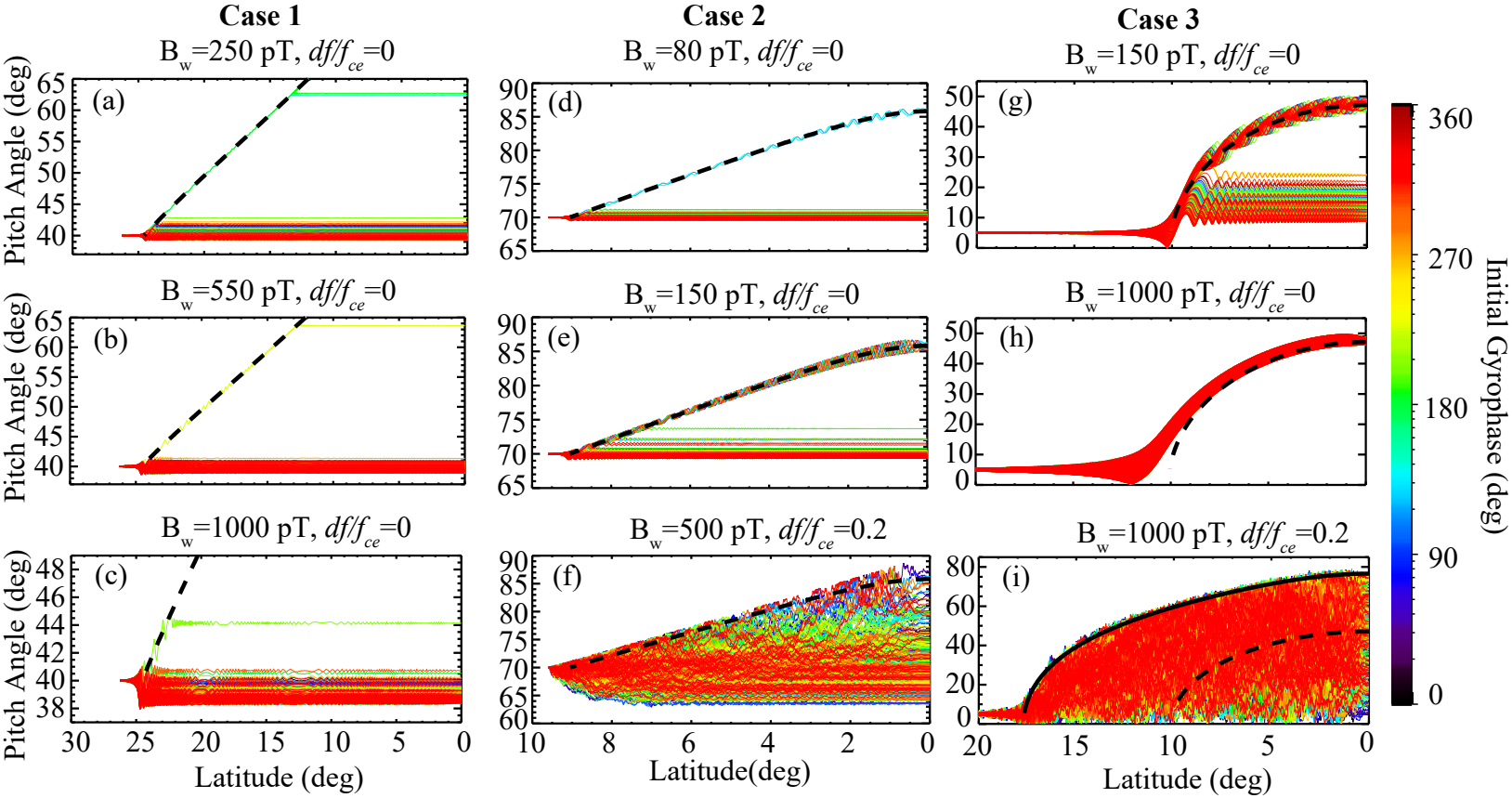
Case 1
Case 2
Case 3
B_w=250 pT, df/f_ce=0
B_w=80 pT, df/f_ce=0
B_w=150 pT, df/f_ce=0
B_w=550 pT, df/f_ce=0
B_w=150 pT, df/f_ce=0
B_w=1000 pT, df/f_ce=0
B_w=1000 pT, df/f_ce=0
B_w=500 pT, df/f_ce=0.2
B_w=1000 pT, df/f_ce=0.2
(a)
(b)
(c)
(d)
(e)
(f)
(g)
(h)
(i)
Pitch Angle (deg)
Latitude (deg)
Latitude(deg)
Initial Gyrophase (deg)
0
90
180
270
360

Figure5.

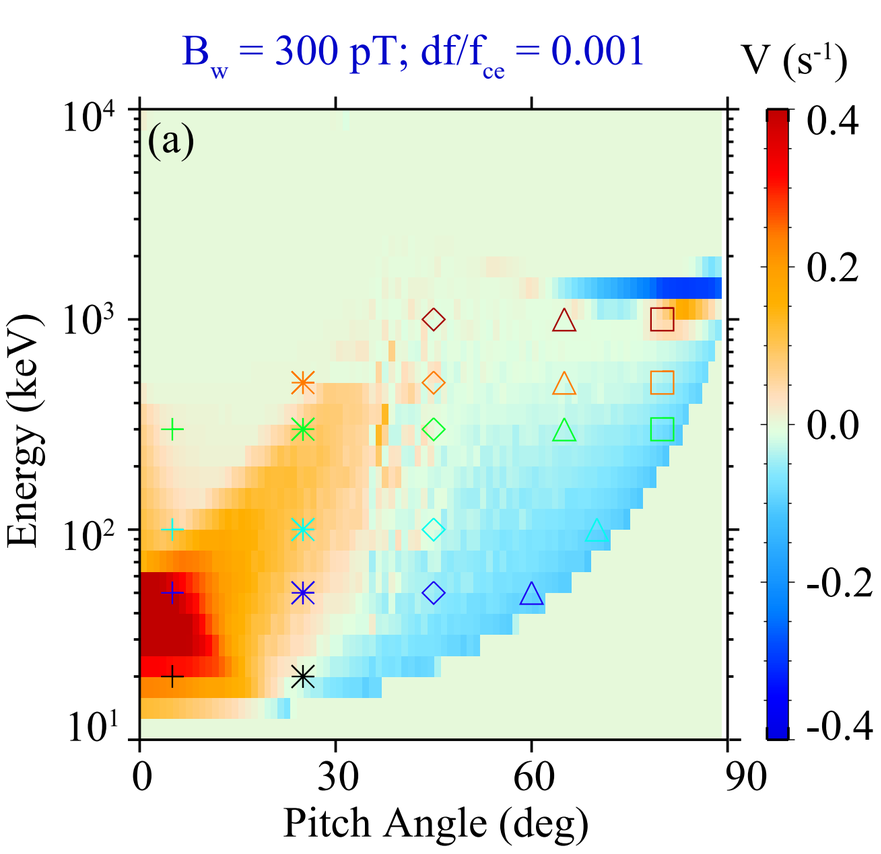

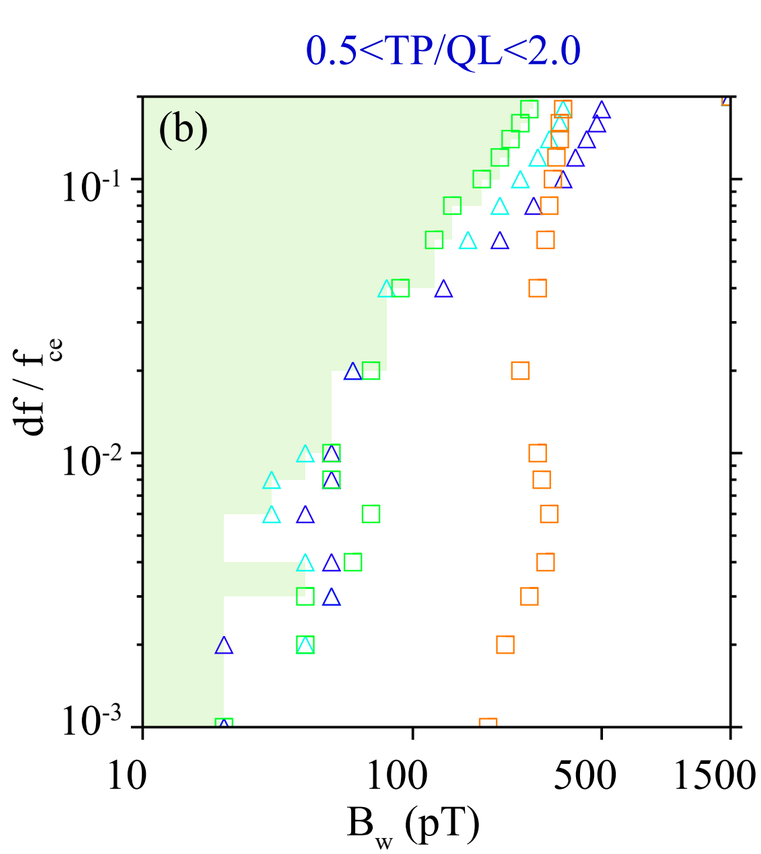

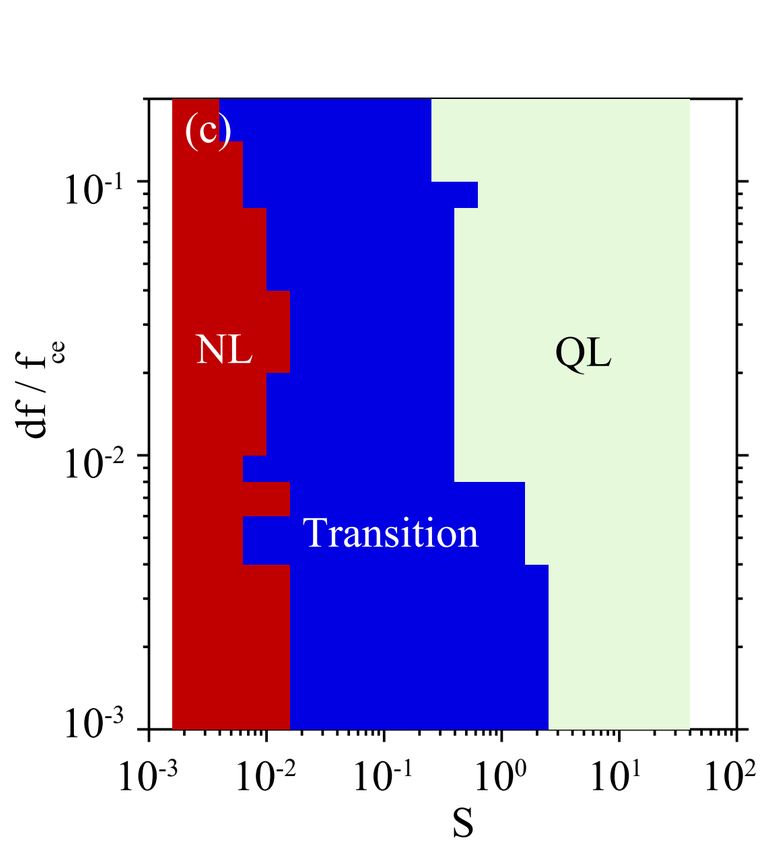
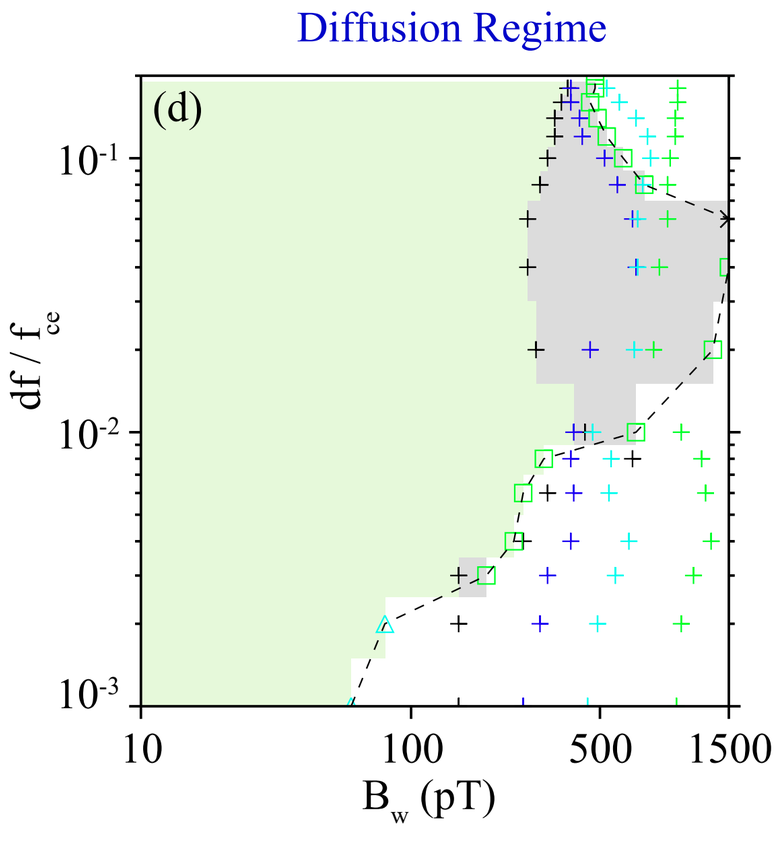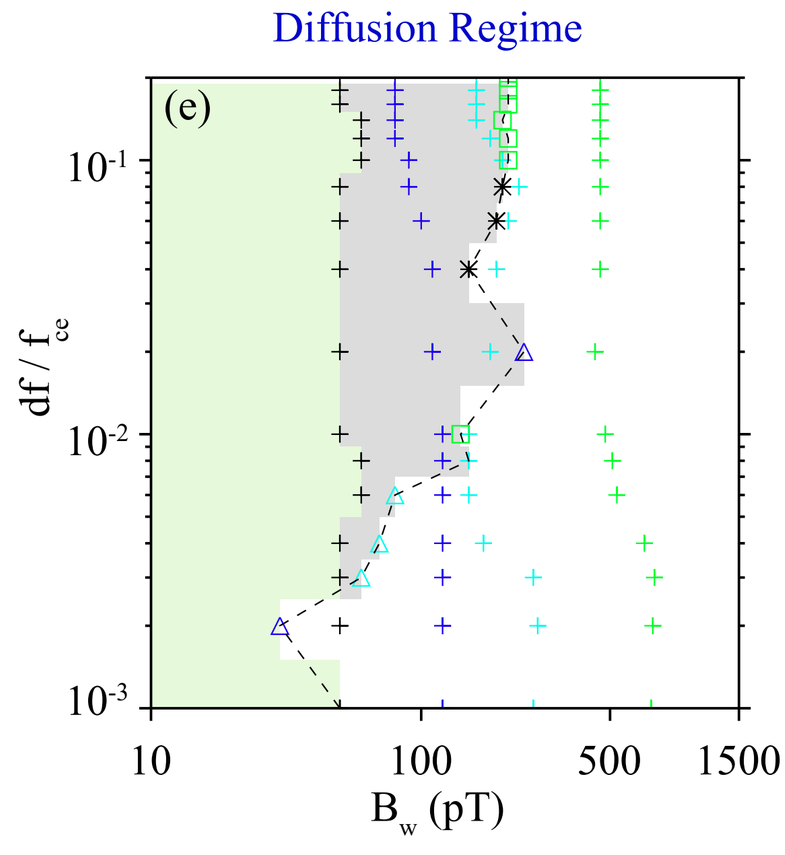
Symbols	PA (deg)	Energy (keV)	S
+	5	20	14.74
✳	25	20	2.13
+	5	50	34.26
✳	25	50	5.39
◇	45	50	1.70
△	60	50	0.46
+	5	100	55.35
✳	25	100	8.41
◇	45	100	2.63
△	70	100	0.41
+	5	300	113.56
✳	25	300	15.10
◇	45	300	3.95
△	65	300	1.63
□	80	300	0.46
✳	25	500	19.16
◇	45	500	4.47
△	65	500	2.16
□	80	500	0.86
◇	45	1000	5.37
△	65	1000	3.38
□	80	1000	1.50